Field Effect Optoelectronic Modulation of Quantum-Confined Carriers in Black Phosphorus

William S. Whitney[1‡], Michelle C. Sherrott[2,3‡], Deep Jariwala[2,3], Wei-Hsiang Lin[2], Hans A. Bechtel[4], George R. Rossman[5], Harry A. Atwater[2,3*]

1. Department of Physics, California Institute of Technology, Pasadena, CA 91125, USA
2. Thomas J. Watson Laboratory of Applied Physics, California Institute of Technology, Pasadena, CA 91125, USA
3. Resnick Sustainability Institute, California Institute of Technology, Pasadena, CA 91125, USA
4. Advanced Light Source, Lawrence Berkeley National Laboratory, Berkeley, CA 94720, USA
5. Division of Geological and Planetary Sciences, California Institute of Technology, Pasadena, CA 91125, USA

‡ Equal contributors

*Corresponding author: Harry A. Atwater (haa@caltech.edu)

Abstract:

We report the infrared optical response of thin black phosphorus under field-effect modulation, and interpret the observed spectral shifts as a combination of an ambipolar Burstein-Moss (BM) bandgap shift due to band-filling and Pauli-blocking under gate control, together with a quantum confined Franz-Keldysh (QCFK) effect, which have been proposed theoretically to occur for BP flakes under electric field modulation. Modulation amplitudes as high as 15% are observed for 25 nm thick layers, suggesting the potential for use of black phosphorus as an active material in mid-infrared optoelectronic modulator applications.

Keywords:

Black phosphorus, tunable optical properties, mid-infrared, Burstein-Moss shift, quantum-confined Franz-Keldysh effect, optical modulator

The emergence of a variety of two-dimensional materials has spurred tremendous research activity in the field of optoelectronics[1-4]. While gapless graphene can in principle exhibit an optoelectronic response at wavelengths ranging from the far infrared to the ultraviolet, its optoelectronic behavior is limited by a lack of resonant absorption and poor optical modulation in the absence of 1D confinement. On the other hand, the semiconducting molybdenum- and tungsten-based transition metal dichalcogenides have shown considerable prospects for visible frequency optoelectronics. Yet while these materials promise exciting new directions for optoelectronics and nanophotonics in visible, they have limited response for lower energy, infrared light.

The isolation of atomically thin black phosphorus in recent years has bridged the wavelength gap between graphene and transition metal dichalcogenides, as black phosphorus is an emerging two-dimensional semiconductor material with an infrared energy gap and typical carrier mobilities between those of graphene and transition metal dichalcogenides.[5-7] Since the first isolation of black phosphorus and demonstration of a field effect device, numerous reports investigating the synthesis and optoelectronic properties of this material have emerged, appropriately summarized in recent reviews.[5, 6, 8, 9] Likewise a number of reports have also appeared on the applications of black phosphorus in fast photodetectors[10], polarization sensitive detectors,[11] waveguide integrated devices[12], multispectral photodetectors[13], heterojunction[14] and split gate p-n homojunction photovoltaics[15], gate-tunable van der Waals heterojunctions for digital logic circuits[16, 17] and gigahertz frequency transistors in analog electronics[18]. A majority of the studies on both the fundamental optical properties of black phosphorus and applications in optoelectronic devices have explored only the visible frequency range[19-22]. Therefore little is known about the intrinsic optical response of black phosphorus in the infrared range. As a narrow band-gap semiconductor, much of the potential for black phosphorus lies in these infrared optoelectronic applications – ranging from tunable infrared emitters[23] and absorbers for waste heat management/recovery[24] to thermophotovoltaics[25] and optical modulators for telecommunications[26]. Theoretical investigations of black phosphorus have suggested novel infrared optical phenomena, such as anisotropic plasmons[27, 28], field-effect tunable exciton stark shifts[29], and strong Burstein-Moss[30] and quantum-confined Franz-Keldysh effects[31] that promise to open new

directions for both fundamental nanophotonics research and applications. In this work, we report the first experimental observations of the infrared optical response of ultrathin BP samples under field effect modulation. We observe modulation of oscillations in the transmission spectra which we attribute to a combination of an ambipolar Burstein-Moss shift / Pauli-blocking effect and quantum-confined Franz-Keldysh behavior. The large modulation of transmittance (up to 15%) we observe in thicker BP (25 nm) suggests promise for BP as an active material in infrared optical modulators.

Measurements were performed on black phosphorous flakes that were mechanically exfoliated in a glove box onto a 285 nm SiO_2/Si substrate. Optical microscope images of these flakes are shown in Figure 1a and 1e. Raman spectroscopy and atomic force microscopy (AFM) (Figures 1b - d and 1e - g) were used to characterize the quality and thicknesses of the samples. Crystal lattice orientations were determined by polarized visible reflectance measurements, as in prior experiments and described in detail in the Supporting Information.[32] We analyzed two flakes of 6.5 nm and 25 nm thickness with lateral dimensions of approximately 10 μm x 10 μm. The observed roughness in AFM scans is attributed primarily to the incomplete removal of a PMMA capping layer prior to the measurement.

A schematic of our experimental setup is shown in Figure 2a. Standard electron beam lithographic and metal deposition methods were used to define Ni/Au electrodes to each exfoliated BP flake. The samples were then immediately coated in PMMA for protection against environmental degradation. Transmission measurements were obtained using a Magna 760 (Nicolet) Fourier Transform Infrared (FTIR) Spectrometer coupled to a NicPlan (Nicolet) infrared microscope on infrared Beamline 1.4.3 at the Advanced Light Source (ALS) at Lawrence Berkeley National Laboratory. This allowed us to perform measurements using a high brightness, diffraction-limited infrared beam, which is necessary for accurately analyzing the small-area BP samples attainable by mechanical exfoliation. The incident light was elliptically polarized due to the synchrotron source, with an intensity ratio of two to one. The major axis and details of the polarization state are indicated and discussed in the Supporting Information. All measurements were done in a Linkam cryo stage at a pressure of 3 mTorr and a temperature of 80 K. First, a gate-dependent source-drain current was measured at 80 K to extract approximate carrier

densities as a function of gate bias. Transmission spectra were then gathered at different gate voltages applied between the flake and lightly doped Si substrate. We note that in our setup, the silicon substrate is grounded and BP experiences the applied voltage, so the sign of the applied voltages is reversed from that in some other works. In order to probe the electric field- and charge-carrier-dependent optical properties of the BP, all spectra were normalized to the zero-bias spectrum. The measured infrared optical properties result primarily from the unique band structure of BP, schematically depicted in Figure 2b. Quantized intersubband transitions provide the primary contribution to its zero-field optical conductivity.

Transport and infrared transmission results for the 6.5 nm thick flake are reported in Figure 3. Transport measurements taken at 80 K and pressure of 3mTorr, shown in Figure 3a, indicate that this sample was heavily hole-doped, and only hole-type transport was observed throughout the voltage sweep of our field-effect device. An on-off ratio of approximately 10^4 was attained, limited by the noise threshold of our measurement (a Keithley 2400 SourceMeter), but consistent with literature values for similar thickness devices[7]. Figure 3b shows the primary result of our experiment, which is the modulated transmission of the sample at different voltages, normalized to the transmission spectrum at zero bias. Three prominent features are observed in these spectra. First, under negative applied bias (i.e.: when the sample is being depleted of holes), a negative peak (I) appears in transmission near 0.45 eV, which grows in amplitude and broadens to lower energies as the magnitude of the bias increases. Second, under positive applied bias (i.e.: when the sample is being increasingly hole-doped), a positive peak (II) appears in transmittance near 0.5-0.7 eV. Lastly, these carrier-dependent effects are superimposed with an oscillatory feature (III) that varies with the magnitude of the applied field, but not its polarity, and which is most clearly visible in the negative bias spectra in the 0.5-0.7 eV range, where no Burstein-Moss shift should be seen.

Due to the distinct character of each feature, we can understand the overall spectral shifts as arising from a combination of a Burstein-Moss (BM) shift and the quantum confined Franz-Keldysh (QCFK) effect, as has been predicted theoretically in BP flakes of this thickness.[31] Because our flake exceeds a thickness of ~4 nm, we can

neglect any excitonic effects and therefore do not consider the giant Stark effect or a normal-to-topological phase transition in our analysis.[21, 22]

We suggest that peak (I) can be described by the onset of allowed j = 1 intersubband transitions as the material is depleted of holes at negative gate voltages, in agreement with our transport measurements. We further suggest that peak (II) can be described primarily by the suppression of j = 2 intersubband transitions as more holes are accumulated in the flake at positive gate voltages. This is shown schematically in Figure 3c. We additionally explain these results by calculating the optical conductivity of our BP flakes at various doping levels, using the theoretical framework developed in ref. [30]. The band structure of thin BP is calculated for various thicknesses and carrier densities and the Kubo formula is used to evaluate the optical conductivity as a function of frequency, shown in Figure 3d. Our experimental results correspond qualitatively in this low energy range to the optical response obtained from our calculations. From these results, we may assign the band gap energy of our flake as being $E_g \sim 0.4$ eV, consistent with theoretical models that predict an increase in band gap energy from the bulk 0.3 eV value as the material thickness decreases to several layers or thinner.[21]

The oscillatory feature (III), on the other hand, grows in magnitude as the local field strength increases, likely corresponding to a shift in the overlap of the first conduction and valence subband wavefunctions as explained by the quantum-confined Franz-Keldysh effect, previously explored theoretically in ref.[31]. In a bulk semiconductor, the Franz-Keldysh effect introduces simple oscillatory perturbations to the absorption edge, but in quantum well structures this behavior is modified.[33] Under a sufficiently strong electric field, hybrid optical transitions between subbands of different index (eg: E_{v1} to E_{c2}) become allowed, even though they are predicted theoretically to be forbidden, and have zero oscillator strength, in the absence of a strong electrostatic field. Notably, recent experimental investigations [34] show evidence that these transitions may still occur without the application of an electric field, and further theoretical and experimental investigation of this phenomenon is needed to fully explain these results. Nonetheless, we suggest that the quantum-confined Franz-Keldysh effect leads to the appearance of the additional oscillatory spectral features we observe, owing to the increased oscillator strength making these transitions significantly more prominent. It is also worthwhile to

note that under a strong applied field, the optical band gap becomes less sharply defined. Interestingly, we see no evidence of a tunable plasma edge; investigations in the long-wave infrared wavelength range with larger samples would likely be needed to observe this feature.

We note that because of the complicated polarization state of incident light from the synchrotron, and because previous studies have extensively studied this effect experimentally[30, 35], we do not study in detail the anisotropic optical properties of BP. However, due to the primary contribution to the optical conductivity arising from the σ_{xx} component, we argue that the only effect of elliptically polarized light is to scale the observed modulation, as discussed in the Supporting Information.

Results for the 25 nm thick BP flake are shown in Figure 4. Unlike the 6.5 nm thick flake, we observe ambipolar transport at a temperature of 80 K and a pressure of 3 mTorr, as shown in Figure 4a. Similar results have been shown in the literature with on/off ratios of ~10^4 for flakes thinner than the one considered here; it is likely that the low operation temperature and strong gate bias conditions used in our experiments, as well as the nearly intrinsic doping of the flake at zero bias enable us to observe strong conductance modulation.[14] The infrared transmission results are shown in Figure 4b, normalized to the zero bias transmission, and show significant modulation of a single broad feature. This feature is strongest at positive bias, and reverses sign twice: it changes polarity as the bias crosses 0 V, and again between -60 V and -120 V.

We interpret our results for the 25 nm sample using a combination of a Burstein-Moss shift and quantum-confined Franz-Keldysh effect. Because this flake exhibits ambipolar transport, we can understand the primary spectral feature as resulting from three separate regimes of charge carrier modulation. At increasingly positive bias (ie: increased hole doping), Pauli blocking of optical transitions is increased, resulting in higher infrared transmission at lower photon energies. At negative bias, transmission first decreases as we deplete the sample of holes and more optical transitions are allowed, and then increases as the sample becomes electron-doped and a Burstein-Moss effect of the opposite charge carrier type is introduced. This ambipolar, gate-controlled Burstein-Moss shift is the first observed in a two-dimensional semiconductor, to the best of our knowledge. We further highlight the significant modulation strength of this effect – a

relative change in transmission of up to 15% despite background signals from the PMMA capping layer and SiO_2/Si substrate.

Superimposed on this large modulation are small oscillations that are most evident at high applied field – particularly +120 V. We suggest that these oscillations are related to features in the quantized intersubband transitions that occur in the BP optical conductivity, as seen from the calculation in Figure 4d. A further, larger oscillation appears in the -120 V transmittance spectrum near 0.3 eV. We speculate that this feature may result from distinctions between electron and hole-doped optical responses; however further study would be required to draw definitive conclusions about this.

In conclusion, we have demonstrated experimentally that ultra-thin black phosphorus exhibits widely tunable optical properties at mid-infrared wavelengths. We find that in 6.5 nm thick BP, modulation of infrared transmission takes place as a result of both a Burstein-Moss shift and quantum confined Franz-Keldysh effect. In thicker 25 nm BP, we observe for the first time an ambipolar Burstein-Moss shift, with modulation strengths up to 15%. While our results verify some of the theoretical predictions about the electro-optical effects in few-layer BP, more work is needed to further understand the BP optical response as function of sample thickness, in addition to the field effect mediated infrared response in the few-layer (< 3 nm) limit. Our results indicate that BP is both an interesting system for exploring the fundamental behavior of quantum confined carriers in two-dimensional semiconductors under field-effect modulation, and a promising candidate for tunable mid-infrared optical devices.

Methods:

BP flakes were exfoliated in a glove box from crystals grown by HQ Graphene. After fabrication of Ni/Au (20 nm / 130 nm) electrodes by electron beam lithography and electron beam evaporation, 90 nm PMMA 950 A2 was spin-coated as an encapsulation layer. Electron beam lithography was again used to expose the contacts for wire bonding. PMMA[8] and other encapsulation layers including ALD grown dielectrics,[36, 37] polymers[38, 39], covalent surface functionalization[40] and atomically thin hexagonal boron nitride[41] have been shown in the past to successfully protect BP devices against ambient degradation.

Acknowledgments:

This work was supported by the U.S. Department of Energy (DOE) Office of Science, under grant DE-FG02-07ER46405. The authors gratefully acknowledge use of the facilities of beamline 1.4.3 at the Advanced Light Source which is supported by the Director, Office of Science, Office of Basic Energy Sciences, of the U.S. Department of Energy under Contract No. DE-AC02-05CH11231. M.C. Sherrott and D. Jariwala acknowledge support by the Resnick Institute and W.S. Whitney acknowledges support by the National Defense Science and Engineering Graduate Fellowship. This research used resources of the National Energy Research Scientific Computing Center, a DOE Office of Science User Facility supported by the Office of Science of the U.S. Department of Energy under Contract No. DE-AC02-05CH11231. The authors are grateful to Victor Brar for helpful discussions.

References:

1. Koppens, F. H. L.; Mueller, T.; Avouris, P.; Ferrari, A. C.; Vitiello, M. S.; Polini, M. *Nature Nanotechnology* **2014,** 9, (10), 780-793.
2. Sun, Z. P.; Martinez, A.; Wang, F. *Nature Photonics* **2016,** 10, (4), 227-238.
3. Wang, Q. H.; Kalantar-Zadeh, K.; Kis, A.; Coleman, J. N.; Strano, M. S. *Nature Nanotechnology* **2012,** 7, (11), 699-712.
4. Xia, F. N.; Wang, H.; Xiao, D.; Dubey, M.; Ramasubramaniam, A. *Nature Photonics* **2014,** 8, (12), 899-907.
5. Castellanos-Gomez, A. *The Journal of Physical Chemistry Letters* **2015,** 6, (21), 4280-4291.
6. Ling, X.; Wang, H.; Huang, S. X.; Xia, F. N.; Dresselhaus, M. S. *P Natl Acad Sci USA* **2015,** 112, (15), 4523-4530.
7. Li, L.; Yu, Y.; Ye, G. J.; Ge, Q.; Ou, X.; Wu, H.; Feng, D.; Chen, X. H.; Zhang, Y. *Nat Nanotechnol* **2014,** 9, (5), 372-7.
8. Du, Y.; Liu, H.; Deng, Y.; Ye, P. D. *ACS Nano* **2014,** 8, (10), 10035-10042.
9. Liu, H.; Du, Y.; Deng, Y.; Ye, P. D. *Chemical Society Reviews* **2015,** 44, (9), 2732-2743.
10. Buscema, M.; Groenendijk, D. J.; Blanter, S. I.; Steele, G. A.; van der Zant, H. S. J.; Castellanos-Gomez, A. *Nano Letters* **2014,** 14, (6), 3347-3352.
11. Yuan, H. T.; Liu, X. G.; Afshinmanesh, F.; Li, W.; Xu, G.; Sun, J.; Lian, B.; Curto, A. G.; Ye, G. J.; Hikita, Y.; Shen, Z. X.; Zhang, S. C.; Chen, X. H.; Brongersma, M.; Hwang, H. Y.; Cui, Y. *Nat Nanotechnol* **2015,** 10, (8), 707-713.
12. Youngblood, N.; Chen, C.; Koester, S. J.; Li, M. *Nat Photonics* **2015,** 9, (4), 247-252.
13. Engel, M.; Steiner, M.; Avouris, P. *Nano Letters* **2014,** 14, (11), 6414-6417.
14. Deng, Y.; Luo, Z.; Conrad, N. J.; Liu, H.; Gong, Y.; Najmaei, S.; Ajayan, P. M.; Lou, J.; Xu, X.; Ye, P. D. *ACS Nano* **2014,** 8, (8), 8292-8299.
15. Buscema, M.; Groenendijk, D. J.; Steele, G. A.; van der Zant, H. S. J.; Castellanos-Gomez, A. *Nat Commun* **2014,** 5.
16. Peng, C.; Jianyong, X.; Hua, Y.; Jing, z.; Guibai, X.; Shuang, W.; Xiaobo, L.; Guole, W.; Jing, Z.; Fusheng, W.; Zhongyuan, L.; Rong, Y.; Dongxia, S.; Guangyu, Z. *2D Materials* **2015,** 2, (3), 034009.
17. Jeon, P. J.; Lee, Y. T.; Lim, J. Y.; Kim, J. S.; Hwang, D. K.; Im, S. *Nano letters* **2016,** 16, (2), 1293-1298.
18. Wang, H.; Wang, X.; Xia, F.; Wang, L.; Jiang, H.; Xia, Q.; Chin, M. L.; Dubey, M.; Han, S.-j. *Nano Letters* **2014,** 14, (11), 6424-6429.
19. Likai Li, J. K., Chenhao Jin, Guojun Ye, Diana Y. Qiu, Felipe H. da Jornada, Zhiwen Shi, Long Chen, Zuocheng Zhang, Fangyuan Yang, Kenji Watanabe, Takashi Taniguchi, Wencai Ren, Steven G. Louie, Xianhui Chen, Yuanbo Zhang and Feng Wang. *arXiv:1601.03103* **2016**.
20. Wang, X. M.; Jones, A. M.; Seyler, K. L.; Tran, V.; Jia, Y. C.; Zhao, H.; Wang, H.; Yang, L.; Xu, X. D.; Xia, F. N. *Nature Nanotechnology* **2015,** 10, (6), 517-521.
21. Tran, V.; Soklaski, R.; Liang, Y. F.; Yang, L. *Phys Rev B* **2014,** 89, (23).
22. Kim, J.; Baik, S. S.; Ryu, S. H.; Sohn, Y.; Park, S.; Park, B. G.; Denlinger, J.; Yi, Y.; Choi, H. J.; Kim, K. S. *Science* **2015,** 349, (6249), 723-6.

23. Brar, V. W.; Sherrott, M. C.; Jang, M. S.; Kim, S.; Kim, L.; Choi, M.; Sweatlock, L. A.; Atwater, H. A. *Nat Commun* **2015,** 6.
24. De Zoysa, M.; Asano, T.; Mochizuki, K.; Oskooi, A.; Inoue, T.; Noda, S. *Nat Photon* **2012,** 6, (8), 535-539.
25. Bermel, P.; Ghebrebrhan, M.; Chan, W.; Yeng, Y. X.; Araghchini, M.; Hamam, R.; Marton, C. H.; Jensen, K. F.; Soljačić, M.; Joannopoulos, J. D.; Johnson, S. G.; Celanovic, I. *Opt. Express* **2010,** 18, (S3), A314-A334.
26. Liu, M.; Yin, X.; Ulin-Avila, E.; Geng, B.; Zentgraf, T.; Ju, L.; Wang, F.; Zhang, X. *Nature* **2011,** 474, (7349), 64-67.
27. Low, T.; Roldán, R.; Wang, H.; Xia, F.; Avouris, P.; Moreno, L. M.; Guinea, F. *Physical Review Letters* **2014,** 113, (10), 106802.
28. Liu, Z.; Aydin, K. *Nano Letters* **2016,** 16, (6), 3457-3462.
29. Chaves, A.; Low, T.; Avouris, P.; Cakir, D.; Peeters, F. M. *Phys Rev B* **2015,** 91, (15).
30. Low, T.; Rodin, A. S.; Carvalho, A.; Jiang, Y.; Wang, H.; Xia, F.; Castro Neto, A. H. *Phys Rev B* **2014,** 90, (7), 075434.
31. Lin, C.; Grassi, R.; Low, T.; Helmy, A. S. *Nano Lett* **2016,** 16, (3), 1683-9.
32. Mao, N.; Tang, J.; Xie, L.; Wu, J.; Han, B.; Lin, J.; Deng, S.; Ji, W.; Xu, H.; Liu, K.; Tong, L.; Zhang, J. *Journal of the American Chemical Society* **2016,** 138, (1), 300-305.
33. Miller, D. A. B.; Chemla, D. S.; Schmitt-Rink, S. *Phys Rev B* **1986,** 33, (10), 6976-6982.
34. Zhang, G.; Chaves, A.; Huang, S.; Song, C.; Low, T.; Yan, H., Infrared fingerprints of few-layer black phosphorus. In *ArXiv e-prints*, 2016; Vol. 1607.
35. Guowei Zhang, A. C., Shenyang Huang, Chaoyu Song, Tony Low,; Yan, H. *arXiv:1607.08049* **2016**.
36. Zhu, W.; Yogeesh, M. N.; Yang, S.; Aldave, S. H.; Kim, J.-S.; Sonde, S.; Tao, L.; Lu, N.; Akinwande, D. *Nano Letters* **2015,** 15, (3), 1883-1890.
37. Wood, J. D.; Wells, S. A.; Jariwala, D.; Chen, K.-S.; Cho, E.; Sangwan, V. K.; Liu, X.; Lauhon, L. J.; Marks, T. J.; Hersam, M. C. *Nano Letters* **2014,** 14, (12), 6964-6970.
38. Favron, A.; Gaufres, E.; Fossard, F.; Phaneuf-Lheureux, A.-L.; Tang, N. Y. W.; Levesque, P. L.; Loiseau, A.; Leonelli, R.; Francoeur, S.; Martel, R. *Nat Mater* **2015,** 14, (8), 826-832.
39. Tayari, V.; Hemsworth, N.; Fakih, I.; Favron, A.; Gaufres, E.; Gervais, G.; Martel, R.; Szkopek, T. *Nat Commun* **2015,** 6.
40. Ryder, C. R.; Wood, J. D.; Wells, S. A.; Yang, Y.; Jariwala, D.; Marks, T. J.; Schatz, G. C.; Hersam, M. C. *Nat Chem* **2016,** 8, (6), 597-602.
41. Doganov, R. A.; O/'Farrell, E. C. T.; Koenig, S. P.; Yeo, Y.; Ziletti, A.; Carvalho, A.; Campbell, D. K.; Coker, D. F.; Watanabe, K.; Taniguchi, T.; Neto, A. H. C.; Ozyilmaz, B. *Nat Commun* **2015,** 6.

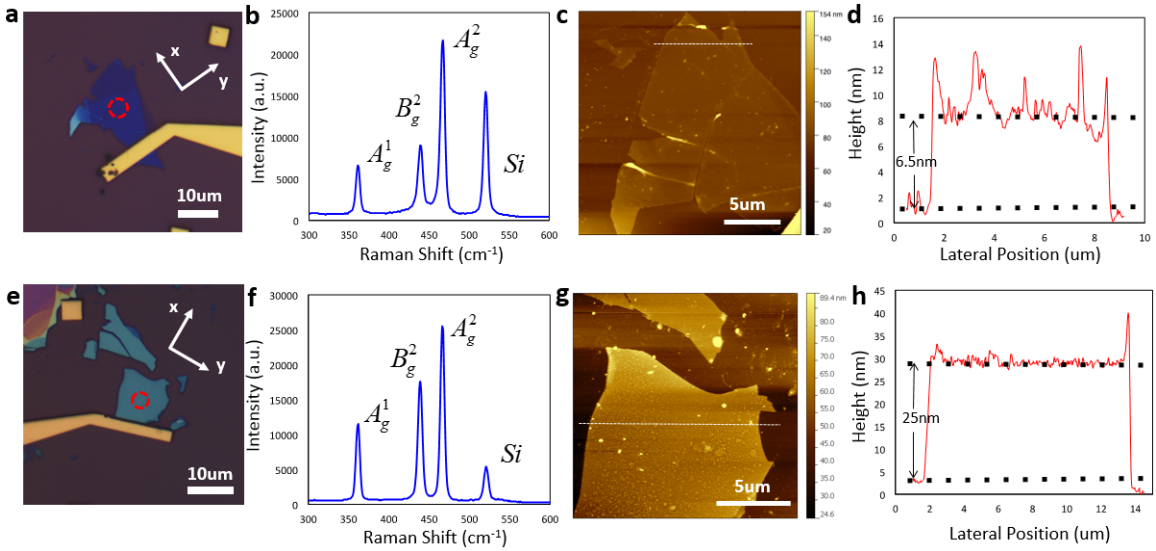

Figure 1: Few-layer black phosphorus sample characterization. **a), e)** Optical image of 6.5 nm and 25 nm black phosphorus flakes, respectively, with red circles indicating the locations of Raman measurements, and white axes indicating directions of the armchair (x) and zig-zag (y) crystal axes. **b), f)** Raman spectrum with characteristic black phosphorus and silicon modes. **c), g)** Large area AFM scans with corresponding cross-cuts **d), h)** Cross-cuts indicating flake thicknesses

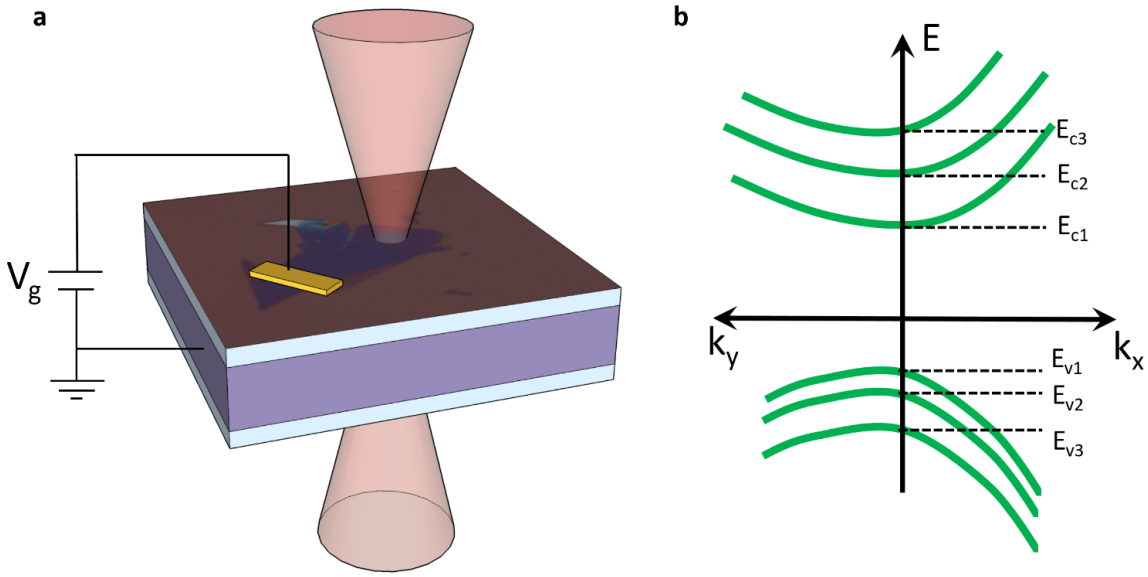

Figure 2: a) Schematic illustration of FTIR transmission modulation experiment. Diffraction-limited IR beam from synchrotron is transmitted through black phosphorus sample. Variable gate voltage applied across SiO_2 modulates transmittance. **b)** Schematic band diagram of few-layer black phosphorus with subbands arising from vertical quantum confinement

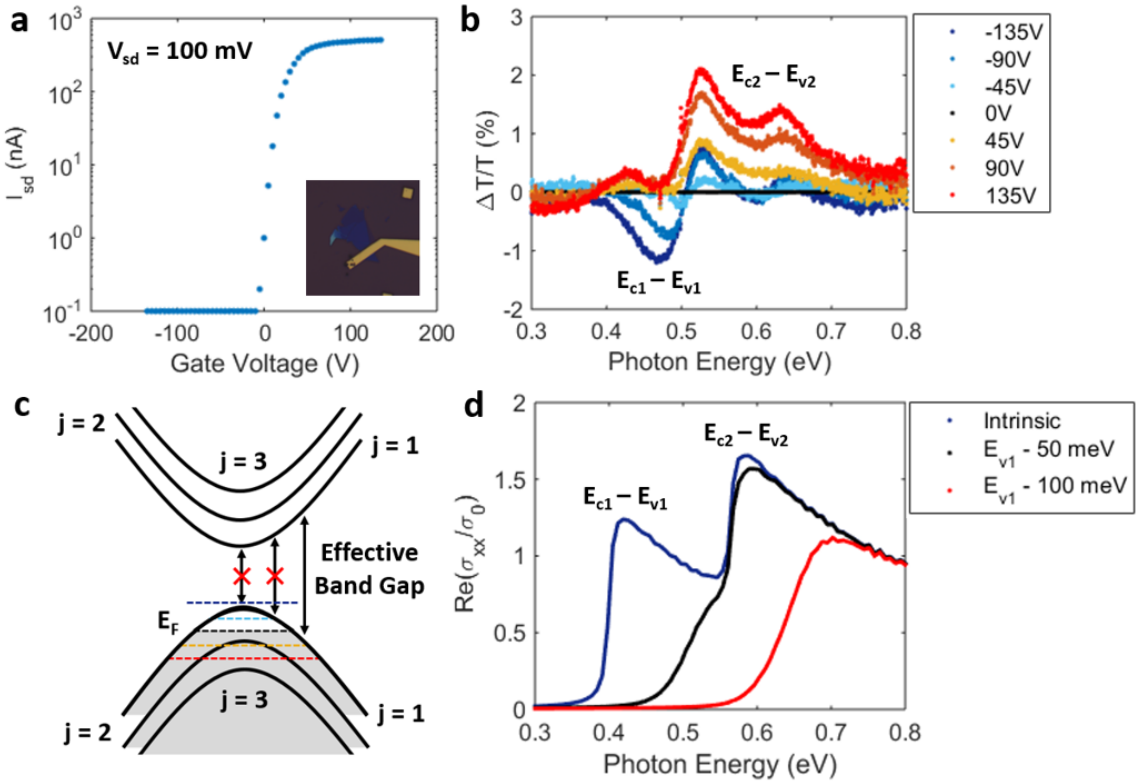

Figure 3: Gate modulation of 6.5 nm flake. **a)** Source-drain current vs gate voltage. Only hole-type conduction is seen. **b)** FTIR transmittance vs photon energy, normalized to zero bias. Peak I noted at E = 0.45 eV, II at 0.6 eV, and III the oscillatory behavior most notable at large biases. **c)** Schematic of electronic band structure and allowed intersubband transitions at different voltages. **d)** Calculated optical conductivity of a 6.5 nm BP flake for different Fermi levels, normalized to the universal conductivity of graphene. Color coding to part **(b)** indicates that the BP is moderately hole doped at zero bias. At negative gate voltages, the previously Pauli-blocked E_{c1}-E_{v1} transition becomes allowed, and at positive gate voltages, the previously allowed E_{c2}-E_{v2} transition is Pauli-blocked. This behavior is superimposed with a field magnitude-dependent effect, which we suggest to be the predicted QCFK effect, and which is clearly visible in the negative voltage spectra above the E_{c1}-E_{v1} transition.

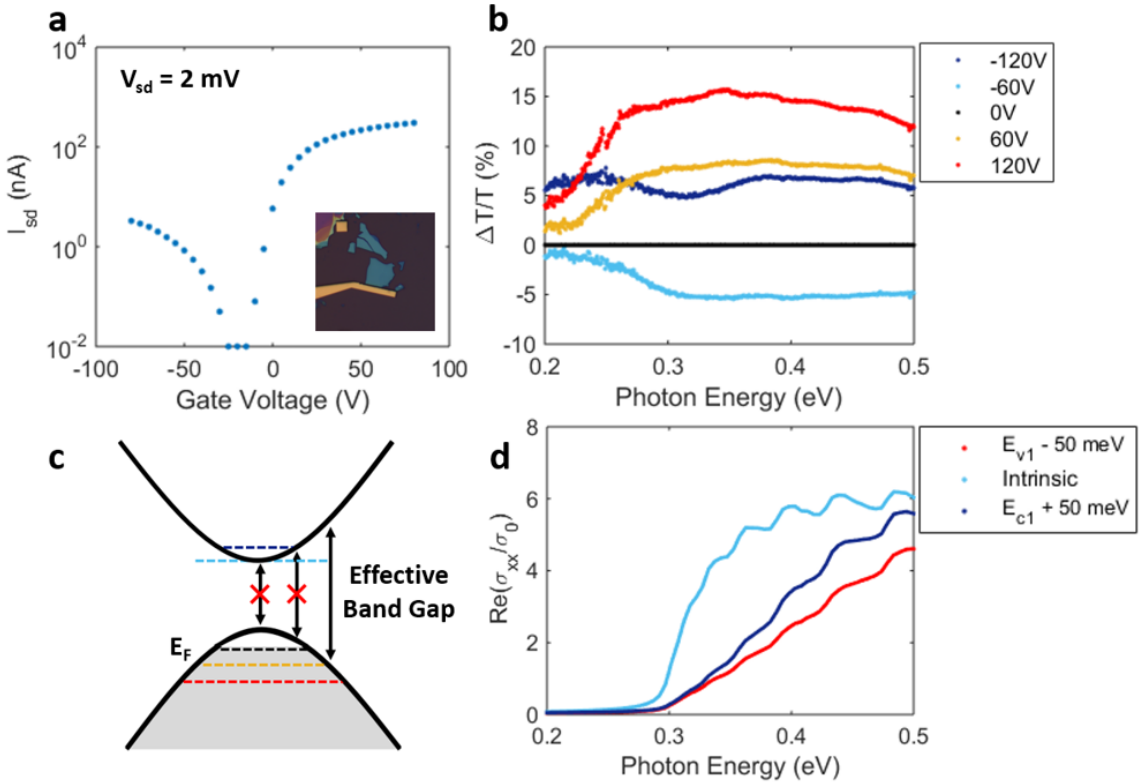

Figure 4: Gate modulation of 25 nm flake. **a)** Source-drain current vs gate voltage. Ambipolar conduction is seen. **b)** FTIR transmittance vs photon energy normalized to zero bias. Gate modulation of up to 15 percent is seen. Small ripples in transmittance are observed, reflecting the quantized optical conductivity. **c)** Schematic of electronic band structure and allowed interband transitions at different voltages. **d)** Calculated optical conductivity of a 25 nm BP flake for different Fermi levels, normalized to the universal conductivity of graphene. Color coding to part (**b)** indicates that the BP is least doped at small negative gate voltage. At larger negative gate voltages, Pauli-blocking reduces the optical conductivity near the band edge, increasing transmittance. At positive gate voltages, Pauli-blocking again reduces the band edge optical conductivity. This behavior suggests an ambipolar Burstein-Moss shift.

Supporting Information for: "Field Effect Optoelectronic Modulation of Quantum-Confined Carriers in Black Phosphorus"

William S. Whitney[1‡], Michelle C. Sherrott[2,3‡], Deep Jariwala[2,3], Wei-Hsiang Lin[2], Hans Bechtel[4], George R. Rossman[5], Harry A. Atwater[2,3*]

1. Department of Physics, California Institute of Technology, Pasadena, CA 91125, USA
2. Thomas J. Watson Laboratory of Applied Physics, California Institute of Technology, Pasadena, CA 91125, USA
3. Resnick Sustainability Institute, California Institute of Technology, Pasadena, CA 91125, USA
4. Lawrence Berkeley National Laboratories, Berkeley, CA 94720, USA
5. Division of Geological and Planetary Sciences, California Institute of Technology, Pasadena, CA 91125, USA

[‡] Equal contributors

*Corresponding author: Harry Atwater (haa@caltech.edu)

I. Crystal Lattice Structure

The x (armchair) and y (zig-zag) crystal lattice directions are determined by polarization-dependent visible reflectance measurements. At each angle of polarization an image is recorded, and pixel RGB values are sampled from both the BP flake and nearby substrate. The ratio of green channel values from flake to substrate is averaged over three sample positions, and plotted as a function of polarization angle in Figure S1. Maxima and minima in green reflectance determine the armchair and zig-zag directions, respectively.[32]

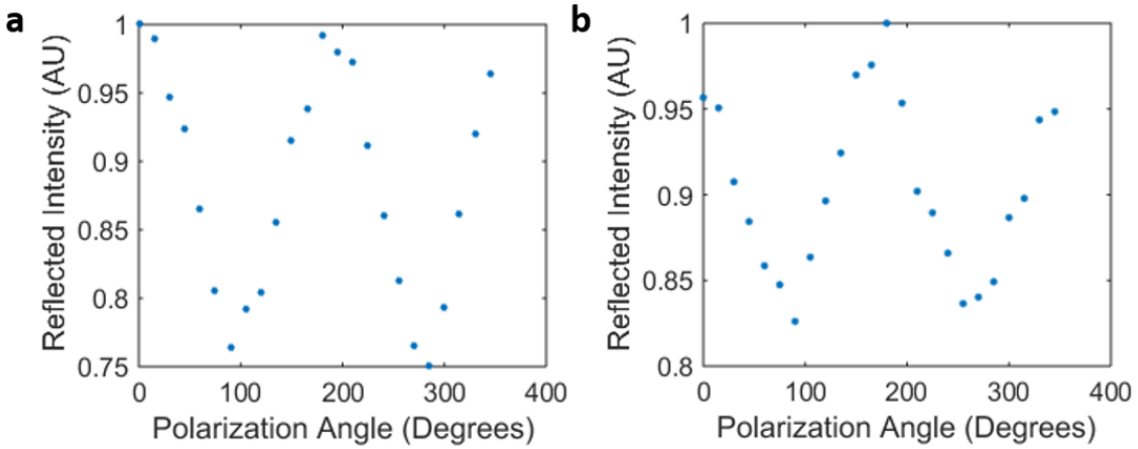

Figure S1: Intensity of the green channel of light reflected from BP flakes as the linear polarization of the incident light is rotated for **a)** the 6.5 nm flake and **b)** the 25 nm flake. In both cases, the polarization angle is defined as the angle between the x (armchair) crystal axis and the linear polarizer. The green component of the pixel RGB of the flakes is normalized to that of the adjacent substrate.

II. Polarization State of FTIR Beam

The FTIR beam used in all transmittance measurements has an inherent elliptical polarization due to its synchrotron source. The polarization state is approximately two to one polarized along the major axis of this ellipse, which is indicated in Figure S2. Due to the complicated polarization state of incident light from the synchrotron, and because previous studies have extensively investigated this effect experimentally[30, 35], we do not study in detail the anisotropic optical properties of BP. However, since the σ_{xx} component of the optical conductivity is one to two orders of magnitude larger than the σ_{yy} component, plotted in Figure S3, we argue that the observed optical response derives almost entirely from light-material interactions along the armchair direction. As a result, the only effect of elliptically polarized light is to scale down the observed modulation strength. Probing devices with light of properly aligned polarization – linear along the armchair direction – would maximize this modulation strength; however, the underlying physics would be unchanged.

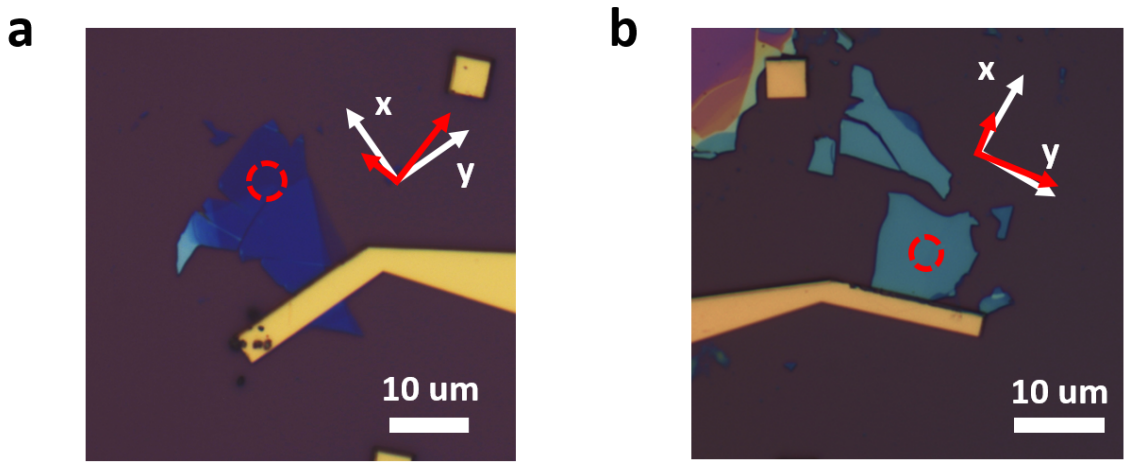

Figure S2: Polarization states of FTIR light. The synchrotron infrared source is inherently polarized at ALS beamline 1.4.3, with a roughly 2:1 elliptical polarization in the direction indicated here in red for **a)** the 6.5 nm flake and **b)** the 25 nm flake. Also indicated are the crystal axes, where x and y correspond to the armchair and zig-zag lattice directions, respectively, and the measurement site, indicated by a red, dashed circle.

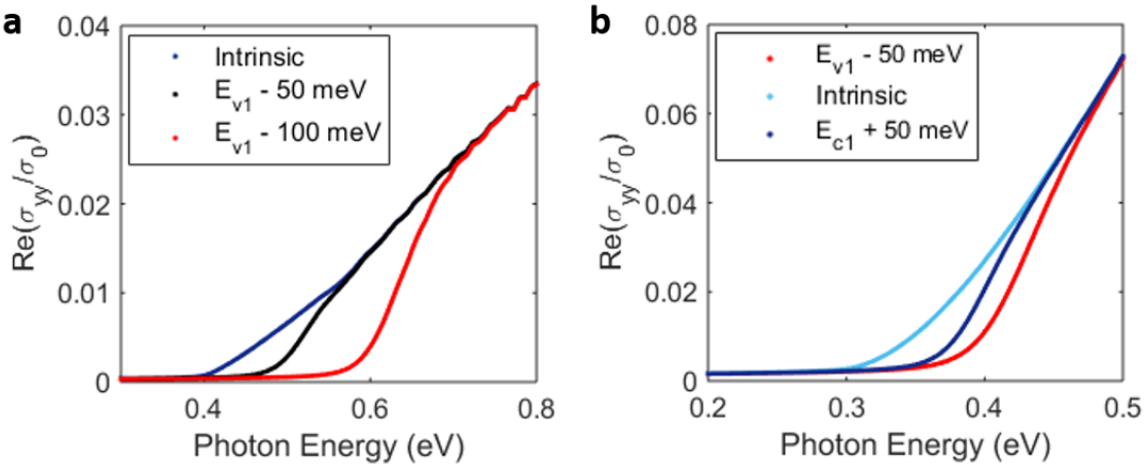

Figure S3: Calculated σ_{yy} optical conductivities at different Fermi levels for **a)** the 6.5 nm flake and **b)** the 25 nm flake. In both cases, σ_{yy} is one to two orders of magnitude smaller than σ_{xx}, implying that the interaction of the FTIR beam with the flake is dominated by the σ_{xx}. As a result, any polarization of the FTIR beam effectively scales the gate modulation as the strength of the interaction of the beam with the σ_{xx} vs σ_{yy} optical conductivity components changes.